Experimental and Statistical Analysis of the Vertical Temperature Gradient, for Ballastless Railway Track, in Alpine and Plateau Environs

Ping Lou[1,2], Tao Shi[1], Weiqi Zheng[1], Xingwang Sheng[1], Chuanshu Li[3], Szabolcs Fischer[4]

[1]School of Civil Engineering, Central South University, Changsha 410075, China

[2]MOE Key Laboratory of Engineering Structures of Heavy-haul Railway, Central South University, Changsha 410075, China

[3]China Railway fifth Bureau Group, Changsha 410000, China

[4]Széchenyi István University, Egyetem tér 1, H-9026 Győr, Hungary

e-mail: pinglou@csu.edu.cn, shitao@csu.edu.cn, wqzheng@csu.edu.cn, shengxingwang@csu.edu.cn, fischersz@sze.hu

Abstract: Temporal temperature evolution of ballastless railway track is a random process caused by complex environmental actions. The vertical temperature gradient (VTG), varying continuously with time, has significant effects on the repeated deformation of ballastless track. However, few researchers have considered the statistical analysis of VTGs in alpine and plateau environs characterized by high altitude, strong solar radiation and high diurnal temperature differences. In this study, a temperature field test platform of ballastless track was established in Shannan City, Tibet and the temperature field of ballastless track was measured. Based on four statistical methods, a Monte Carlo simulation (MCS), Gaussian mixture model (GMM), Generalized Pareto distribution (GPD) and a third-order polynomial normal transformation technique (TPNT), the VTGs of ballastless track in alpine and plateau areas, are statistically analyzed. The results show that the applied statistical methods, used for predicting the VTG representative value, in ballastless track, are feasible within different application conditions. The recommended positive and negative representative values of the VTG of ballastless track are 91.58 °C/m and -40.15 °C/m, and 82.83 °C/m and -35.03 °C/m, with failure probabilities of 1% and 5% respectively, in alpine and plateau areas. The research results can provide a reference for the design and maintenance of ballastless track used in alpine and plateau environs.

Keywords: Ballastless track; Temperature distribution; Long-term field test; Vertical temperature gradient; alpine and plateau environs; Statistical analysis

1 Introduction

The high-speed railways, due to their high transportation capacity, environmental friendliness, and safe operation, have been the latest trend for railway developments all over the world [1] [2]. Among them, the Southwest Plateau Railway is of great significance to China's 13th Five-Year Plan, which subsequently climbs 5000 m and runs across the Tibetan plateau [3] [4]. The alpine and plateau environs generally experience high levels of solar radiation, low rainfall, and large diurnal temperature variation [5]. The effects of the complex alpine plateau climatic environment on the construction of the Southwest Plateau Railway should not be ignored.

Ballastless tracks with high stability, small settlements, and low maintenance have been widely utilized and developed in the construction of the Southwest Plateau Railway, but the damage of them cannot be avoided during their service life. Ballastless tracks with large material property differences and complex climatic variations, were vulnerable to various degrees of damage in the complex service environment [6]. The effects of temperature loads on the interface damage evolution process of ballastless tracks have been analyzed [7] [8]. The damage characteristics of ballastless track structures were related to deformation imbalance caused by thermal loads, and various degrees of the arch at the joints between prefabricated slabs were produced under non-uniform temperature distributions [9]. The problems of ballastless track structures have been analyzed combined with the effect of temperature increase and positive temperature gradient [10]. The damage of ballastless tracks under time-varying service environments was closely related to the effects of temperature gradients. Therefore, the study of temperature gradients has significant effects on the optimization design, maintenance, and damage control of ballastless tracks in alpine and plateau environs.

Many pieces of research focused on temperature distributions in concrete structures exposed to various environmental actions [11]. The heat transfer analysis of ballastless tracks has been conducted to calculate the non-uniform temperature distributions and vertical temperature gradients based on meteorological data such as solar radiation and environmental temperature [6] [12]. The vertical temperature gradient and temperature variation of ballastless tracks in natural environment have been investigated, based on field test and temperature simulation [13] [14]. The variation trend of temperature field evolvement and temperature gradient of ballastless tracks has been studied considering the geographical locations and environmental conditions [15] [16]. Based on the meteorological data, the nonlinear temperature distribution and temperature gradients of ballastless tracks obey certain statistical regularity [17]. Because meteorological conditions change all the time, the statistical characteristics of temperature gradients of ballastless tracks are varied. Thus, the statistical analysis of the temperature gradient in ballastless tracks exposed to alpine plateau climatic conditions deserves to be studied in detail.

The statistical analysis of temperature gradients, in different structures considering environmental conditions, has been concerned by many researchers. Effective extreme value analysis has been proposed to establish the most unfavourable temperature gradient of concrete-filled steel tubes [18]. The statistical characteristic of maximum or minimum temperature differences has been described by the Gaussian mixture model of flat-steel-box girders and truss girders [19]. Temperature action representative values in a bridge-track system have been researched through a statistical method of a virtual distribution built by high-order moments of data [20]. Based on the stationary binomial probability model, the vertical temperature gradient models and transverse temperature gradient models of concrete box girder have been determined [21] [22]. In the existing studies, the statistical analysis of a certain mathematical model applied to VTG in different structures has been concerned [23]. However, the application of different statistical methods is various under different monitoring periods and analysis objectives. The comparative analysis of different statistical methods for predicting VTG of ballastless track in alpine and plateau environs warrants further detailed study.

In this study, based on the long-term temperature field test of ballastless track in Shannan City, Tibet, the statistical methods including MCS, GMM, GPD, and TPNT, are used to investigate the VTG variation trend of ballastless track considering complex alpine plateau climatic. The VTG representative values with different failure probabilities are analyzed based on the four statistical methods. Furthermore, the recommended positive and negative representative values of VTG of ballastless track are determined.

2 Experimental Program

2.1 Experimental Setup

The temperature distribution of ballastless track influenced by atmospheric temperature, wind speed, altitude, and climatic conditions vary continuously with time. The site construction of the ballastless track located in Gongga County, Shannan City, Tibet Autonomous Region, China (N29.25˚, E92.21˚) was shown in Figure 1. The ballastless track is situated in the plateau climatic zone (mountainous area), with an air pressure of 61.3 kPa and an altitude of 3535 m.

The length and width of the ballastless track were 4.0 m and 2.8 m, respectively, and the interval between supporting block tracks was 0.65 m. The centerline of the ballastless track was in the direction of northeastern 23˚, and the plane layout of the ballastless track was described in Figure 2. Section A-A was the middle section of the ballastless track, where temperature measuring sensors were arranged.

)a) Concrete pouring of ballastless track

)b) Concrete maintenance of ballastless track

Figure 1
The ballastless track used on site

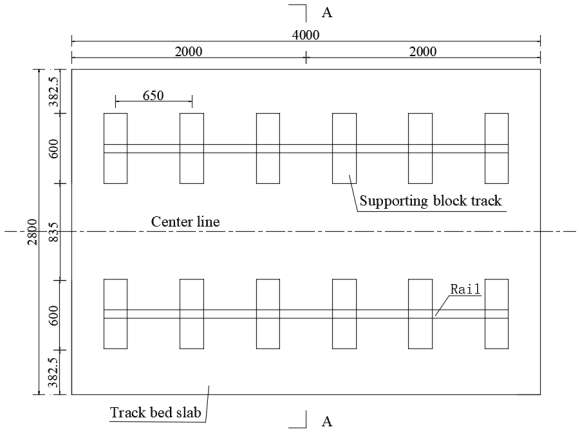

Figure 2
The plane layout of ballastless track (unit: mm)

2.2 Experimental Procedure

The monitoring period of the long-term field test was from 00:19:10 on January 31, 2021 to 03:19:10 on March 1, 2022, with a sampling frequency of 0.5 hours. Thermometers were arranged on the A-A section of ballastless track, to obtain the temperature variation trend of ballastless track in Gongga County. The VTGs of ballastless track were analyzed, and the VTG representative values of ballastless track with different failure probabilities were determined. Structural dimensions and layout of thermometers of ballastless track were shown in Figure 3.

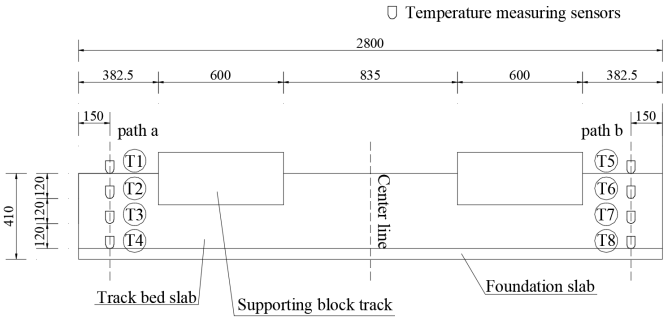

Figure 3
Structural dimensions and layout of thermometers (unit: mm)

From Figure 3, the thermometers T1, T2, T3, and T4 were arranged on the path a of ballastless track, and the thermometers T5, T6, T7, and T8 were arranged on path b of ballastless track. The thermometers T1 and T5 were arranged on the top edge of ballastless track, and the thermometers T4 and T8 were arranged on the bottom edge of ballastless track. The arrangement of thermometers and the data acquisition system were shown in Figure 4.

(a) Thermometers on the top edge of the ballastless track

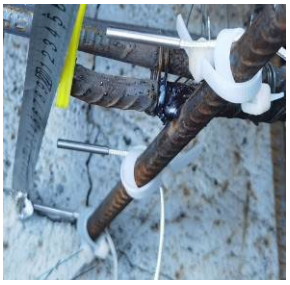

(b) Thermometers embedded in the ballastless track

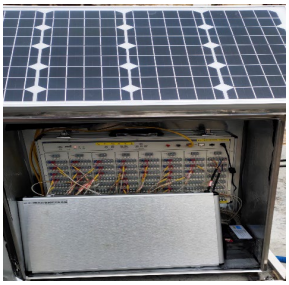

(c) Data acquisition system powered by solar energy

Figure 4
The arrangement of thermometers in ballastless track and data acquisition system

From Figure 4, thermometers were arranged on the top edge of ballastless track and embedded in ballastless track, respectively, to obtain the temperature distribution of ballastless track. Thermometers YC-PT1000/3 with the accuracy ±0.1 ºC and measurement ranging from -85 ºC to 300 ºC, were used to monitor the temperature variations of ballastless track and atmospheric. Based on the temperature monitoring data of ballastless track, the non-uniform temperature distribution, and the temporal and spatial temperature variation of ballastless track were put forward.

2.3 Experimental Results

In this experiment, the temperature variations along path a and b of the ballastless track from January 31, 2021 to March 1, 2022 were investigated. Except for several data missing due to instrumental failure, most of the temperature data has been obtained via the monitoring system. The temperature evolutions along path a and b of the ballastless track were shown in Figure 5.

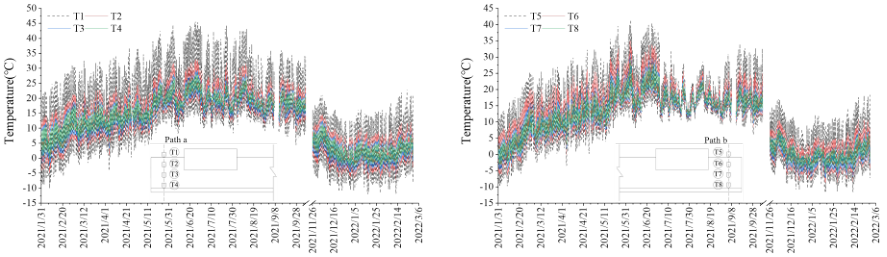

)a) Temperature variation along path a)b) Temperature variation along path b

Figure 5
Temperature variations of the ballastless track

From Figure 5, the temperature variation trend along path a and b of the ballastless track were almost the same. The temperature variation of sensor T1 along path a ranged from -12.06 ºC to 45.61 ºC, and the temperature variation of sensor T5 along path b ranged from -11.76 ºC to 41.45 ºC. The temperature variation trend along path a varied more drastically than that of path b. Due to the heat transfer laws of concrete materials, the evolution of the internal temperature of the ballastless track lags behind the edge temperature of the ballastless track [24]. The VTG of the track slabs is $(T_{\varphi} - T_{\beta}) / D$, where T_{φ} is the temperature of the top edge in the track slabs; T_{β} is the temperature of the bottom edge in the track slabs; and D is the track slabs thickness (0.24 m). The VTG of ballastless track can provide an important reference for their design and maintenance, and the variation trend of VTGs (path a) and air temperature were shown in Figure 6.

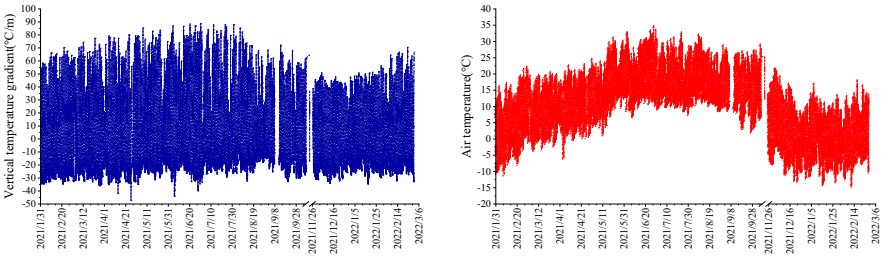

)a) Variation trend of VTGs along path a)b) Variation trend of air temperature

Figure 6
Comparison of the VTG in the ballastless track

From Figure 6, the variation characteristics of VTGs and air temperature were almost the same. The VTGs of ballastless track varied from -47.16 °C/m to 88.88 °C/m, and the atmospheric temperature varied from -13.81 °C and 35.09 °C. Furthermore, the distribution characteristics of VTGs were described and the VTG representative values with different failure probabilities were predicted based on various statistical methods.

3 Statistical Analysis

Because the most unfavourable VTGs of ballastless track occurred in the summer and winter of the long-term field test period from January 31, 2021 to March 1, 2022, the temperature experiment could reflect the statistical characteristics of a year. The temperature distribution of ballastless track showed temporal and spatial variation characteristics with the change of measured position and time, and the VTG representative values could be analyzed using statistical methods. Positive and negative daily extreme VTG along path a obtained from the long-term temperature field test were set as random variables, respectively. Statistical methods including MCS, GMM, GPD, and TPNT were used to describe the distribution characteristics of ballastless track' VTGs and predict the VTG representative value R_q with a failure probability q of 5%.

3.1 Monte-Carlo Simulation

Monte Carlo simulation is a method of repeated random sampling based on Bernoulli's law of large numbers, to predict the VTG representative values in ballastless track with different failure probabilities [25]. The positive daily extreme VTG sample set S, with a size of n_p ($n_p = 339$) was sampled randomly for W(W=10^9) times, and the sample set S^* could be obtained, where $S^* = \{S_1^*, S_2^*, ..., S_W^*\}$. The performance function was defined as $G_i^* = R - S_i^*$, where R was the initial ultimate value; and the set G^* was determined by sampling randomly, where $G^* = \{G_1^*, G_2^*, ..., G_W^*\}$. The VTG positive representative value R_q with different failure probabilities q of the ballastless track could be expressed in Eq. (1):

$$q = \frac{\sum_{i=1}^{W} L(G_i^*)}{W} \tag{1}$$

where: $L(x) = \begin{cases} 1 & x \le 0 \\ 0 & x > 0 \end{cases}$; and W is the number of random experiments. The failure frequency of VTG in the ballastless track was conducted in

W (W=10^9) random experiments, and the VTG positive representative value R_q with different failure probabilities q of the ballastless track could be calculated and shown in Figure 7.

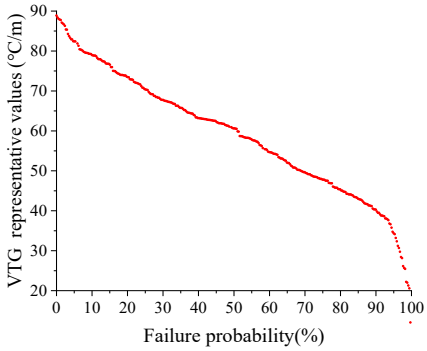

Figure 7

The VTG positive representative values with different failure probabilities

From Figure 7, the VTG positive representative values decreased with the increase of the failure probabilities. When the number of random experiments was large enough, the failure frequency of VTG was convergent to the failure probability of VTG. The VTG representative values showed nonlinear characteristics when the failure probability was less than 5% and more than 95%, because the statistical analysis of MCS was sensitive to the tail data of VTG sample. When the failure probability was between 5% and 95%, the VTG representative values were linearly correlated with failure probabilities. The VTG representative value with a failure probability of 5% was calculated in Eq. (2):

$$\frac{\sum_{i=1}^{10^9} L(R_{5\%} - S_i^*)}{10^9} = 5\% \tag{2}$$

Based on this, the VTG positive representative value of ballastless track in alpine and plateau environs was 82.41 °C/m with a failure probability of 5%. According to the same calculation principle, the VTG negative representative value of ballastless track was -34.13 °C/m with a failure probability of 5%.

3.2 Gaussian Mixture Model

The temperature distribution of ballastless track can be accurately described by GMM defined in Eq. (3), which is a statistical method composed of several Gaussian distributions [26].

$$f(X|\theta) = \sum_{l=1}^{L} \alpha_l \phi(X \mid \theta_l) \tag{3}$$

where α_l is the weight coefficient of the l^{th} Gaussian distribution ($\alpha_l \geq 0$ and $\sum_{l=1}^{L} \alpha_l = 1$); L is the number of combinations of Gaussian distribution; and $\phi(X \mid \theta_l)$ is the probability density function of the l^{th} Gaussian distribution, described in Eq. (4).

$$\phi(X \mid \theta_l) = \frac{1}{\sqrt{2\pi}\sigma_l} \exp(-\frac{(X-\mu_l)^2}{2\sigma_l^2}) \tag{4}$$

where θ_l is equal to (μ_l, σ_l^2); μ_l is the mean of the l^{th} Gaussian distribution; and σ_l^2 is the variance of the l^{th} Gaussian distribution. Based on the Expectation-maximization algorithm and Kolmogorov-Smirnov test, the parameters of the GMM $\theta=(\alpha_1, \alpha_2, ..., \alpha_l; \theta_1, \theta_2, ..., \theta_L)$ were estimated [27, 28]. When L was 4, significance level α was 0.05 and sample size was n_p, *KS* statistic D in Eq. (5) was 0.019 smaller than the critical value $D(n, \alpha)$, and the null hypothesis where the sample random variable X came from GMM failed to be rejected [29]. The statistical characteristics of VTG sample were described using GMM in Eq. (6):

$$D = \max_{1 \leq j \leq n} | F_N(X_j) - F_{N0}(X_j) | \tag{5}$$

Where X_j is the j^{th} VTG sample (with $j = 1, 2, ..., n$); F_N is the empirical cumulative distribution function; and F_{N0} is the cumulative distribution function of the VTG sample.

$$f(X|\theta) = \alpha_1 \phi(X \mid \theta_1) + \alpha_2 \phi(X \mid \theta_2) + \alpha_3 \phi(X \mid \theta_3) + \alpha_4 \phi(X \mid \theta_4) \tag{6}$$

where α_1=0.251 , $\alpha_2 = 0.098$, $\alpha_3 = 0.332$, $\alpha_4 = 0.320$; and θ_1=(77.70, 31.06) , $\theta_2 = (34.55, 91.14)$, $\theta_3 = (63.34, 22.70)$, $\theta_4 = (47.59, 30.10)$.

Based on this, the probabilistic histogram and probability density function of GMM was obtained as shown in Figure 8.

From Figure 8, the variation trend of probabilistic histogram and probability density function of GMM was almost the same, so the statistical characteristics of VTG in the ballastless track could be described by the GMM. Based on the trial algorithm and probability density function of the GMM, the VTG positive representative value R_q with different failure probabilities q in the ballastless track could be defined in Eq. (7):

$$q = \frac{\int_{R_q}^{+\infty} f(X) dX}{\int_{0}^{+\infty} f(X) dX} \tag{7}$$

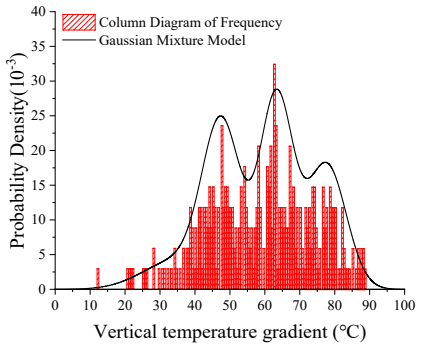

Figure 8
Distribution of vertical temperature gradient

Based on this, the VTG positive representative value of ballastless track in alpine and plateau environs was 82.41 °C/m with a failure probability of 5%. According to the same calculation principle, the VTG negative representative value of ballastless track was -34.56 °C/m with a failure probability of 5%.

3.3 Generalized Pareto Distribution

The GPD is a function of predicting the tail data of test sample that is beyond a position parameter, which can be expressed in Eq. (8):

$$P(X>u)=\begin{cases}1-(1+\xi\dfrac{X-u}{\sigma})^{-1/\xi} & \xi\neq 0\\ 1-\exp(-\dfrac{X-u}{\sigma}) & \xi=0\end{cases} \tag{8}$$

where u is the position parameter; ξ is the shape parameter; and σ is the scale parameter [30]. The VTG representative values of different failure probabilities of the ballastless track could be predicted by GPD [31]. In detail, the VTG samples were divided into $m(m=399)$ groups of independent samples according to the interval of Δt (1 day). The maximum VTG value X_i in each group was determined, which belonged to the maximum value set $\{X_i\}(i=1,2,...,m)$, and the set of order statistics $\{X_{\mathrm{i}}^*\}$ could be obtained by sorting the maximum value set, where $X_1^*\le X_2^*\le...\le X_m^*$. The empirical cumulative probability function of order statistics was defined in Eq. (9):

$$\hat{F}(X_{\mathrm{i}}^*)=F(X\le X_{\mathrm{i}}^*)=i/(m+1)=i/400 \quad (1\le i\le 400) \tag{9}$$

Based on Minimum Squared Error, BoostStarp Method, and Trial Method, the size k of tail order statistic set was obtained and the sample S_1 was composed of tail order statistic, where $S_1=\{X_{m-k+1}^*-u, X_{m-k+2}^*-u,..., X_m^*-u\}$. The position

parameter u was described in Eq. (10), and the shape parameter ξ_0 of the sample S_1 was calculated in Eq. (11):

$$u=\mathrm{X}^{*}_{m-k} \tag{10}$$

$$\xi_0=0.5(1-\frac{E^2(S_1)}{\mathrm{var}(S_1)}) \tag{11}$$

The sample-set Z was determined by repeated random sampling for k numbers from the sample S_1, which was carried out p times, and the shape parameter ξ_z of sample set Z was computed, where $\xi_z=\{\xi_1,\xi_2,...,\xi_p\}$. The bias, variance, and mean square error of the shape parameter ξ_z were expressed from Eq. (12) to Eq. (14), respectively:

$$\mathrm{bias}(\xi_z)=\mathrm{E}(\xi_z)=\frac{1}{p}\sum_{i=1}^{p}\xi_i-\xi_0 \tag{12}$$

$$\mathrm{var}(\xi_z)=\frac{1}{p\text{-}1}\sum_{i=1}^{p}(\xi_i-\frac{1}{p}\sum_{j=1}^{p}\xi_j)^2 \tag{13}$$

$$\mathrm{MSE}(\xi_z)=\mathrm{bias}^2(\xi_z)+\mathrm{var}(\xi_z) \tag{14}$$

When the size k, position parameter u, shape parameter ξ, and empirical cumulative probability $\hat{F}(u)$ of the tail order statistic set were 20, 81.88, -0.61, and 0.94, respectively, the mean square error of the tail order statistic set was the minimum, where $\mathrm{MSE}(\xi)=0.23$, and k, u, ξ, and $\hat{F}(u)$ were the optimal estimation results. When the shape parameter ξ is less than zero, the real shape parameter ξ tends to be zero. Thus, the shape parameter ξ was revised to zero with the modified GPD determined, and the scale parameter σ of the tail order statistic set was described in Eq. (15):

$$\sigma=0.5E(\mathrm{S}_1)(\frac{E^2(S_1)}{\mathrm{var}(S_1)}+1) \tag{15}$$

Based on this, the cumulative probability function of the random variable X of VTG, and the VTG representative value R_q with different failure probabilities $\mathrm{q}(\mathrm{q}\le 11\%)$ of the ballastless track were computed in Eq. (16) and Eq. (17):

$$F(X)=\begin{cases}\hat{F}(X) & X\le u\\ \hat{F}(u)+[1-\hat{F}(u)][1-\exp(-\frac{X-u}{\sigma})] & X>u\end{cases} \tag{16}$$

$$R_{\mathrm{q}} = u - \sigma \ln(1 - \frac{(1\text{-q}) - \hat{F}(u)}{1 - \hat{F}(u)}) \tag{17}$$

where $u = 81.88$, σ=5.48, and $\hat{F}(u) = 0.94$. Based on this, the probabilistic histogram and probability density function of GPD with the random variable X larger than 81.88 were expressed and shown in Figure 9.

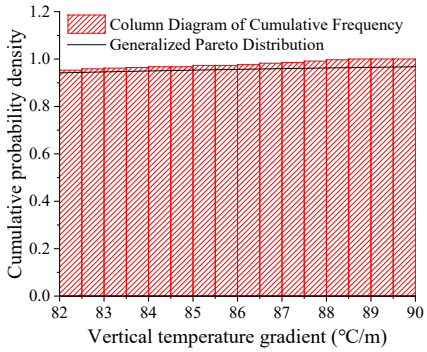

Figure 9
Distribution of vertical temperature gradient

From Figure 9, the probabilistic histogram and probability density function of GPD with the random variable X larger than 81.88 were almost the same, and the statistical characteristics of VTGs in the ballastless track were described by GPD ($X > u$). The VTG representative values were conservative because the probability density function of GPD was lower than the probabilistic histogram of VTG. Based on this, the VTG positive representative value of ballastless track in alpine and plateau environs was 82.77 ºC/m with a failure probability of 5%. According to the same calculation principle, the VTG negative representative value of ballastless track was -34.25 ºC/m with a failure probability of 5%.

3.4 Third-Order Polynomial Normal Transformation Technique

The evolution characteristics of VTGs in the ballastless track are described by the third-order polynomial normal transformation method, based on the definition of the probability moment without empirical judgment [32]. The first four moments (i.e., the mean, standard deviation, skewness, and kurtosis) of the VTG sample S of the ballastless track were calculated in Eq. (18) and Eq. (19) [33]:

$$\mu_S = \frac{1}{n}\sum_{j=1}^{n} X_j, \sigma_S = \sqrt{\frac{1}{n-1}\sum_{j=1}^{n}(X_j - \mu_S)} \tag{18}$$

$$\alpha_{rS}\sigma_S^r = \frac{1}{n-1}\sum_{j=1}^{n}(X_j - \mu_S)^r, r = 3,4 \tag{19}$$

where μ_S, σ_S, α_{3S}, and α_{4S} were the mean, standard deviation, skewness, and kurtosis of the VTG sample S, respectively. The distribution variation of VTGs was analyzed, and the first four moments of the VTG samples of μ_S, σ_S, α_{3S}, and α_{4S} were 59.096, 15.123, -0.218, and 2.546, respectively. The first four moments (μ_G, σ_G, α_{3G}, and α_{4G}) of the performance function $Z = G(X)=R-S$ can be obtained by μ_S, σ_S, α_{3S}, and α_{4S}, which can be described in Eq. (20):

$$\mu_G=R-59.096, \sigma_G=15.123, \alpha_{3G}=-0.218, \alpha_{4G}=2.546 \tag{20}$$

The performance function $Z = G(X)$ can be standardized using its mean and standard deviation, and the standardized performance function Z_G was approximated by a third-order polynomial of the standard normal random variable u, which was expressed in Eq. (21) and Eq. (22) [34]:

$$Z_G = \frac{G(X)-\mu_G}{\sigma_G} \tag{21}$$

$$Z_G = \mathrm{F}(u,\mathbf{M})=a_1 + a_2u + a_3u^2 + a_4u^3 \tag{22}$$

where $\mathbf{M}$ was the vector denoting the first four moments of the performance function $Z = G(X)$. The coefficients of a_1, a_2, a_3, and a_4 were described from Eq. (23) to Eq. (26) [35] [36]:

$$a_1 + a_3 = 0 \tag{23}$$

$$a_2^2 + 2a_3^2 + 6a_2a_4 + 15a_4^2 = 1 \tag{24}$$

$$6a_2^2a_3 + 8a_3^3 + 72a_2a_3a_4 + 270a_3a_4^2 = \alpha_{3G} \tag{25}$$

$$\begin{aligned} &3(a_2^4 + 20a_2^3a_4 + 210a_2^2a_4^2 + 1260a_2a_4^3 + 3465a_4^4) \\ &+12a_3^2(5a_2^2 + 5a_3^2 + 78a_2a_4 + 375a_4^2) = \alpha_{4G} \end{aligned} \tag{26}$$

With the skewness α_{3G} and kurtosis α_{4G} of the performance function known, the standardized performance function Z_G was expressed in Eq. (27), and the distribution characteristics of u and Z_G were shown in Figure 10:

$$Z_G = F(u,\mathbf{M}) = -0.045 + 1.097u + 0.045u^2 - 0.035u^3 \tag{27}$$

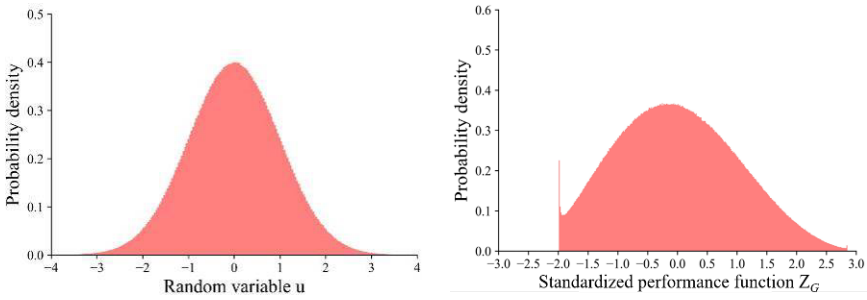

(a) The distribution of random variable u (b) The distribution of Z_G

Figure 10
The distribution of random variable u and standardized performance function Z_G

From Figure 10, the distribution variation of the standardized performance function Z_G was different from that of the random variable u. The distribution of Z_G was asymmetric, and the probability density of negative Z_G was higher than that of positive Z_G. The ballastless track was in the limit or failure state when the performance function Z was less than or equal to zero. The VTG representative value R_q with different failure probabilities q can be determined in Eq. (28):

$$\begin{aligned} q &= \text{Prob}(G(X) \le 0) = \text{Prob}(\sigma_G Z_G + \mu_G \le 0) \\ &= \text{Prob}(Z_G \le -\frac{\mu_G}{\sigma_G}) = \text{Prob}(Z_G \le -\beta_{2M}) \end{aligned} \tag{28}$$

where β_{2M} equal to μ_G / σ_G was the second-order second-moment reliability index [37]. Based on Trial Method, the VTG positive representative value of ballastless track in alpine and plateau environs was 82.83 ºC/m with a failure probability of 5%. According to the same calculation principle, the VTG negative representative value of ballastless track was -35.03 ºC/m with a failure probability of 5%.

4 Discussions

In this study, MCS, GMM, GPD, and TPNT have been conducted to analyze the VTG representative values with the failure probability of 5% of the ballastless track. The VTG representative values with different failure probabilities were obtained, and the comparisons of the four statistical methods are shown in Table 1 and Table 2.

Table 1
VTG positive representative values (unit: ºC/m)

Failure probability (%)	Recommended values	MCS	GMM	GPD	TNPT
1	91.58	87.82	87.47	91.58	87.89
2	87.78	86.66	85.54	87.78	86.32
5	82.83	82.41	82.41	82.77	82.83
10	79.14	78.90	79.14	78.97	78.79
Average relative error (%)			0.50	1.53	0.28

Table 2
VTG negative representative values (unit: ºC/m)

Failure probability (%)	Recommended values	MCS	GMM	GPD	TNPT
1	-40.15	-40.15	-39.71	-38.98	-39.63
2	-37.69	-36.04	-37.38	-36.77	-37.69
5	-35.03	-34.13	-34.56	-34.25	-35.03
10	-32.87	-32.86	-32.72	-32.60	-32.87
Average relative error (%)			1.62	1.52	2.14

Based on large random experiments (10^9 times), the VTG representative values in MCS tend to be accurate. From Table 1 and Table 2, the average relative error (ARE) of the VTG representative values in GMM, GPD, and TPNT was 1.26% compared with MCS, verifying that these statistical methods can predict the VTG representative values with different failure probabilities.

The deviation of statistical results was influenced by the different calculation principles of these statistical methods. MCS has high requirements for the discretization degree and the data scale of VTG sample. When the accuracy of MCS was required to be less than 0.1%, the number of repeated random sampling of the VTG sample needs to be more than 10^5 times. The calculation accuracy of GMM was high (ARE of 1.06%), but the statistical automation of GMM (subjective randomness inevitable) cannot be realized with the prediction process being complex and tedious. The statistical results of GPD were sensitive to the tail data of VTG samples and difficult to be stable. Furthermore, the calculation accuracy of TNPT depended on the distribution of standardized performance function, and it was an automatic computation technique avoiding haphazard and subjectivity.

The VTG representative values obtained by the four statistical methods were deviated, and the recommended representative values of VTG should be conservative, considering the safety and reliability of ballastless track. As seen in Table 1 and Table 2, the recommended representative values of VTG were the maximum representative values among these statistical methods. The positive and

negative VTG representative values of 91.58 ºC/m and -40.15 ºC/m are larger than that of 90 ºC/m and -45 ºC/m in China High Speed Railway Design Code. The positive VTG value in China High Speed Railway Design Code is not conservative for ballastless track design in alpine and plateau areas. Based on this, the recommended positive and negative representative values of VTG of ballastless track were 91.58 ºC/m and -40.15 ºC/m, and 82.83 ºC/m and -35.03 ºC/m, with failure probabilities of 1% and 5% respectively in alpine and plateau environs.

Conclusions

In this study, various statistical analysis tools were employed, using MCS, GMM, GPD and TPNT, to describe the evolution characteristics of the VTGs in a ballastless railway track system, based on the long-term temperature field test of ballastless track in Shannan City, Tibet. The VTG representative values with various failure probabilities are investigated and the statistical results from the above mentioned statistical tools, are examined. The main conclusions are as follows:

1) Based on the long-term temperature field test, the temperature variation of ballastless track in alpine and plateau environs has been studied. The temperature variation of the ballastless track ranged from -12.06 ºC to 45.61 ºC, and the VTG of the track slab ranged from -47.16 ºC /m to 88.88 ºC /m from January 31, 2021 to March 1, 2022, in alpine and plateau environs.

2) These statistical methods are feasible to predict the representative value of VTG of the ballastless track with different failure probabilities. The deviation of these statistical results is caused by the different calculation principles and application conditions of these statistical methods.

3) MCS has high requirements for the discretization degree and the data scale of VTG sample. The statistical automation of GMM cannot be realized with subjective randomness inevitable and prediction process tedious. The statistical results of GPD are sensitive to the tail data of VTG samples. Furthermore, TPNT is an automatic computation technique avoiding haphazard subjectivity.

4) The recommended positive and negative representative values of VTG of ballastless track are 91.58 ºC/m and -40.15 ºC/m, and 82.83 ºC/m and -35.03 ºC/m, with failure probabilities of 1% and 5% in alpine and plateau areas. The positive VTG value in China High Speed Railway Design Code is not conservative for ballastless track design, in alpine and plateau environments.

Acknowledgments

The authors are grateful to projects (52078501, 52078490, 52078488) supported by the National Natural Science Foundation of China, and the Natural Science Foundation of Hunan Province (2022JJ40628).

References

[1] Chen L. K., Kurtulus A., Dong Y. F., Taciroglu E., Jiang L. Z.: Velocity pulse effects of near-fault earthquakes on a high-speed railway vehicle-ballastless track-benchmark bridge system, Vehicle System Dynamics, 2021; 1-25, https://doi.org/10.1080/00423114.2021.1933546

[2] Kurhan M. B., Kurhan D. M., Husak M. A., Hmelevska N.: Increasing the efficiency of the railway operation in the specialization of directions for freight and passenger transportation, Acta Polytechnica Hungarica, 2022; 19(3): 231-244, https://10.12700/APH.19.3.2022.3.18

[3] Lu C. F., Cai C. X.: Challenges and countermeasures for construction safety during the Sichuan-Tibet railway project, Engineering, 2019; 5(5), https://doi.org/10.1016/j.eng.2019.06.007

[4] Fischer S.: Investigation of the horizontal track geometry regarding geogrid reinforcement under ballast. Acta Polytechnica Hungarica, 2022; 19(3): 89-101, https://10.12700/APH.19.3.2022.3.8

[5] Xue Y. G., Kong F. M., Li S. C., Zhang Q. S., Qiu D. H., Su M. X., Li Z. Q.: China starts the world's hardest "Sky-High Road" project: Challenges and countermeasures for Sichuan-Tibet railway, The Innovation, 2021; 2(2): 100105, https://doi.org/10.1016/j.xinn.2021.100105

[6] Song L., Liu H. B., Cui C. X., Yu Z. W, Li Z. G.: Thermal deformation and interfacial separation of a CRTS II slab ballastless track multilayer structure used in high-speed railways based on meteorological data, Construction and Building Materials, 2020; 237: 117528, https://doi.org/10.1016/j.conbuildmat.2019.117528

[7] Zhu S. Y., Cai C. B.: Interface damage and its effect on vibrations of slab track under temperature and vehicle dynamic loads, International Journal of Non-Linear Mechanics, 2014; 58: 222-232, https://doi.org/10.1016/j.ijnonlinmec.2013.10.004

[8] Zhang J. W., Zhu S. Y., Cai C. B., Wang M. Z., Li H. L.: Experimental and numerical analysis on concrete interface damage of ballastless track using different cohesive models, Construction and Building Materials, 2020; 263: 120859, https://doi.org/10.1016/j.conbuildmat.2020.120859

[9] Cai X. P, Luo B. C, Zhong Y. L., Zhang Y. R., Hou B. W.: Arching mechanism of the slab joints in CRTSII slab track under high temperature conditions, Engineering Failure Analysis, 2019; 98: 95-108, https://doi.org/10.1016/j.engfailanal.2019.01.076

[10] Li Y., Chen J. J., Wang J. X., Shi X. F., Chen L.: Study on the interface damage of CRTS II slab track under temperature load, Structures, 2020; 26: 224-236, https://doi.org/10.1016/j.istruc.2020.04.014

[11] Sheng X. W., Zhou T. M., Huang S. J., Cai C. Z., Shi T.: Prediction of Vertical Temperature Gradient on Concrete Box-girder Considering Different Locations in China, Case Studies in Construction Materials, 2022; e01026, https://doi.org/10.1016/j.cscm.2022.e01026

[12] Sheng X. W., Shi T., Zheng W. Q., Lou P.: Time-varying non-uniform temperature distributions in concrete box girders caused by solar radiation in various regions in China, Advances in Mechanical Engineering, 2022; 14(2): 16878140221076458, https://doi.org/10.1177/16878140221076458

[13] Shi T., Lou P.: Optimized machine learning approaches for identifying vertical temperature gradient on ballastless track in natural environments, Construction and Building Materials, 2023; 367: 130321, https://doi.org/10.1016/j.conbuildmat.2023.130321

[14] Shi T., Lou P., Zheng W. Q., Sheng X. W.: A hybrid approach to predict vertical temperature gradient of ballastless track caused by solar radiation, Construction and Building Materials, 2022; 352: 129063, https://doi.org/10.1016/j.conbuildmat.2022.129063

[15] Fu J., Qin Y., You Y. Y., Meng J. Y., Lian X. L.: Temperature field analysis on CA mortar ballastless track of high-speed railway, Key Engineering Materials, 2013; 531: 163-167, https://doi.org/10.4028/www.scientific.net/KEM.531-532.163

[16] Yang R. S., Li J. L., Kang W. X., Liu X. Y., Cao S. H.: Temperature characteristics analysis of the ballastless track under continuous hot weather, Journal of Transportation Engineering, 2017; 143(9): 04017048, https://doi.org/10.1061/JTEPBS.0000076

[17] Yu Z. W., Xie Y., Tian X. Q.: Research on mechanical performance of CRTS III plate-type ballastless track structure under temperature load based on probability statistics, Advances in Civil Engineering, 2019; 2019, https://doi.org/10.1155/2019/2975274

[18] Liu J., Liu Y. J., Zhang G. J.: Experimental analysis of temperature gradient patterns of concrete-filled steel tubular members, Journal of Bridge Engineering, 2019; 24(11): 04019109, https://doi.org/10.1061/(ASCE)BE.1943-5592.0001488

[19] Wang G. X., Ding Y. L., Liu X. W.: The monitoring of temperature differences between steel truss members in long-span truss bridges compared with bridge design codes, Advances in Structural Engineering, 2019; 22(6): 1453-1466, https://doi.org/10.1177/1369433218815436

[20] Lou P., Zhu J. P., Dai G. L., Yan B.: Experimental study on bridge–track system temperature actions for Chinese high-speed railway, Archives of Civil and Mechanical Engineering, 2018; 18(2): 451-464, https://doi.org/10.1016/j.acme.2017.08.006

[21] Song Z. W., Xiao J. Z., Shen L. M.: On temperature gradients in high-performance concrete box girder under solar radiation, Advances in Structural Engineering, 2012; 15(3): 399-415, https://doi.org/10.1260/1369-4332.15.3.399

[22] Cai C. Z., Huang S. J., He X. H., Zhou T. M., Zou Y. F.: Investigation of concrete box girder positive temperature gradient patterns considering different climatic regions, Structures, 2022; 35: 591-607, https://doi.org/10.1016/j.istruc.2021.11.030

[23] Shi T., Sheng X. W., Zheng W. Q., Lou P.: Vertical temperature gradients of concrete box girder caused by solar radiation in Sichuan-Tibet railway, Journal of Zhejiang University-SCIENCE A, 2022; 23(5): 375-387, https://doi.org/10.1631/jzus.A2100401

[24] Sheng X. W., Yang Y., Zheng W. Q., Zhou B., Li S., Huang L. C.: Study on the time-varying temperature field of small radius curved concrete box girder bridges, AIP Advances, 2020; 10(10): 105013, https://doi.org/10.1063/1.5133992

[25] Zio E.: The Monte Carlo simulation method for system reliability and risk analysis, London: Springer, 2013; 19-58

[26] Mclachlan G. J., Rathnayake S.: On the number of components in a Gaussian mixture model, Wiley Interdisciplinary Reviews: Data Mining and Knowledge Discovery, 2014; 4(5): 341-355, https://doi.org/10.1002/widm.1135

[27] Chen Y. H., Gupta M. R.: Em demystified: An expectation-maximization tutorial, Electrical Engineering, 2010

[28] Do C. B., Batzoglou S.: What is the expectation maximization algorithm, Nature biotechnology, 2008; 26(8): 897-899, https://doi.org/10.1038/nbt1406

[29] Frank J., Massey J.: The Kolmogorov-Smirnov test for goodness of fit, Journal of the American statistical Association, 1951; 46(253): 68-78

[30] Fan Z. Y., Huang Q., Ren Y., Xu X., Zhu Z. Y.: Real-time dynamic warning on deflection abnormity of cable-stayed bridges considering operational environment variations, Journal of performance of constructed facilities, 2021; 35(1): 04020123, https://doi.org/10.1061/(ASCE)CF.1943-5509.0001537

[31] Xu X., Ren Y., Huang Q., Fan Z. Y., Tong Z. J., Chang W. J., Liu B.: Anomaly detection for large span bridges during operational phase using structural health monitoring data, Smart Materials and Structures, 2020; 29(4): 045029, https://doi.org/10.1088/1361-665X/ab79b3

[32] Zhao Y. G., Ono T.: Moment methods for structural reliability, Structural safety, 2001; 23(1): 47-75, https://doi.org/10.1016/S0167-4730(00)00027-8

[33] Zhao Y. G., Ono T.: New point estimates for probability moments, Journal of Engineering Mechanics, 2000; 126(4): 433-436, https://doi.org/10.1061/(ASCE)0733-9399(2000)126:4(433)

[34] Chen X. Y., Tung Y. K.: Investigation of polynomial normal transform, Structural Safety, 2003; 25(4): 423-445, https://doi.org/10.1016/S0167-4730(03)00019-5

[35] Zhao Y. G., Lu Z. H.: Cubic normal distribution and its significance in structural reliability, Structural Engineering and Mechanics, 2008; 28(3): 263-280, https://doi.org/10.12989/sem.2008.28.3.263

[36] Zhao Y. G., Lu Z. H.: Fourth-moment standardization for structural reliability assessment, Journal of Structural Engineering, 2007; 133(7): 916-924, https://doi.org/10.1061/(ASCE)0733-9445(2007)133:7(916)

[37] Lu Z. H., Hu D. Z., Zhao Y. G.: Second-order fourth-moment method for structural reliability, Journal of Engineering Mechanics, 2017; 143(4): 06016010, https://doi.org/10.1061/(ASCE)EM.1943-7889.0001199